

Superhydrophobic drag reduction in laminar flows: a critical review

Choongyeop Lee¹  · Chang-Hwan Choi² · Chang-Jin Kim³

Received: 9 August 2016 / Accepted: 9 October 2016 / Published online: 19 November 2016
© The Author(s) 2016. This article is published with open access at Springerlink.com

Abstract A gas in between micro- or nanostructures on a submerged superhydrophobic (SHPo) surface allows the liquid on the structures to flow with an effective slip. If large enough, this slippage may entail a drag reduction appreciable for many flow systems. However, the large discrepancies among the slippage levels reported in the literature have led to a widespread misunderstanding on the drag-reducing ability of SHPo surfaces. Today we know that the amount of slip, generally quantified with a slip length, is mainly determined by the structural features of SHPo surfaces, such as the pitch, solid fraction, and pattern type, and further affected by secondary factors, such as the state of the liquid–gas interface. Reviewing the experimental data of laminar flows in the literature comprehensively and comparing them with the theoretical predictions, we provide a global picture of the liquid slip on structured surfaces to assist in rational design of SHPo surfaces for drag reduction. Because the trapped gas, called plastron, vanishes along with its slippage effect in most application conditions, lastly we discuss the recent efforts to prevent its

loss. This review is limited to laminar flows, for which the SHPo drag reduction is reasonably well understood.

1 Introduction

1.1 Slip on smooth surfaces

The rapid development of nano- and microfluidic systems brought a renewed attention to the solid–liquid boundary condition during the last decade (Neto et al. 2005; Bocquet and Barrat 2007). If channels are nanometers or micrometers in diameter, even a small amount of slip on their inner surfaces was expected to ease the fluid transport appreciably. The amount of slip is best quantified using slip length, which is defined as the ratio of slip velocity to shear rate at the wall or a virtual distance into the wall at which the liquid velocity vanishes to zero when linearly extrapolated (Fig. 1a). It is commonly agreed upon that the slip length on smooth hydrophobic surfaces is less than tens of nanometers while that on hydrophilic surfaces is effectively zero or undetectably small (Choi et al. 2003; Lauga et al. 2005; Neto et al. 2005).

1.2 Slip length, length scale of flows, and drag reduction

For the slip on a surface to reduce drag enough for engineering importance, the slip length δ needs to be comparable to the characteristic length scale of the flow. For example, the drag reduction (DR) by a liquid slip in Couette flow is calculated to be $DR = 1/(1 + H/\delta)$, where H is the gap distance between the slip surface and the opposing nonslip surface (Choi and Kim 2006a). A similar expression of $DR = 3/(3 + H/\delta)$ has been derived for Poiseuille flow (Ou

✉ Choongyeop Lee
cylee@khu.ac.kr

Chang-Hwan Choi
cchoi@stevens.edu

Chang-Jin Kim
cjkim@ucla.edu

¹ Department of Mechanical Engineering, Kyung Hee University, Yongin, Gyeonggi 446-701, Korea

² Department of Mechanical Engineering, Stevens Institute of Technology, Hoboken, NJ 07030, USA

³ Mechanical and Aerospace Engineering Department, University of California at Los Angeles (UCLA), Los Angeles, CA 90095, USA

et al. 2004; Choi et al. 2006). According to these expressions, as a rule of thumb, a drag reduction of $\sim 10\%$ is expected when the slip length is 10% of the characteristic length scale of the flow system, e.g., the channel height for channel flows. For a given slip length, i.e., for a given wall surface, the amount of drag reduction would increase if the channel becomes smaller. Even the mere tens of nanometers of slip length on smooth hydrophobic surfaces would be meaningful in nanofluidic systems whose length scale (e.g., channel diameter) is nanometers (Holt et al. 2006). However, for regular (large-scale) fluidic applications, such as boats, whose viscous boundary layer thickness is on the order of a millimeter, the first-order estimate indicates a slip length on the order of $100\ \mu\text{m}$ would be necessary to obtain an appreciable ($>10\%$) drag reduction. This level of slip length (order of $100\ \mu\text{m}$) is several orders of magnitude larger than what is possible on smooth hydrophobic surfaces (order of 10 nm), explaining why they have not been useful to reduce the drag of water vehicles or pressure drop of common pipe flows. While the eventual interest is in drag reduction, in this review we will focus on the slip length to avoid the effect of flow system on drag reduction and ensure a fair comparison between different slip surfaces.

1.3 Large effective slip on superhydrophobic surfaces

Let us imagine a liquid flowing over a solid surface covered with a uniform gas layer, as illustrated in Fig. 1b. If the thickness of the gas layer is h and liquid and gas viscosities are given by η_{liquid} and η_{gas} , the effective slip length δ can be calculated by assuming continuity of shear stress at the liquid–gas interface: $\delta = h(\eta_{\text{liquid}}/\eta_{\text{gas}} - 1)$. A slip length of $50\ \mu\text{m}$ is expected if the gas layer is 1- μm -thick air in water at room temperature (Choi et al. 2006). However, this ideal configuration is only hypothetical, as a uniform gas film is thermodynamically unstable and cannot be sustained. On the other hand, pockets of gas can be stably

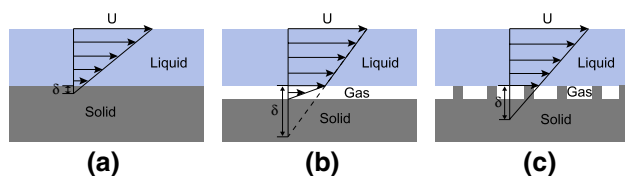


Fig. 1 Liquid flow over a solid surface with a slip quantified as slip length (δ). **a** A liquid flows over a hydrophobic solid surface with a negligibly small (tens of nanometers) slip length. **b** If hypothetically there exists a gas layer between a liquid and a solid, a liquid would flow with a large effective slip length because the gas has a much lower viscosity than the liquid. **c** When a composite interface with solid and gas is formed on a structured surface, a liquid may flow with an effective slip length approaching that of **(b)**

maintained in between surface structures made of a non-wettable material, as schematically shown in Fig. 1c. As the liquid–solid contacts on top of the structures will impart a nonslip skin friction, the effective slip length cannot be as large as that on the uniform gas layer with the same thickness (Fig. 1b). Nevertheless, the slip enhancement was found significant compared with smooth surfaces (Watanabe et al. 1999; Kim et al. 2002; Ou et al. 2004; Choi and Kim 2006a; Choi et al. 2006), propelling the superhydrophobic (SHPo)¹ surfaces of Fig. 1c as a potential drag-reducing surface for fluidic systems above micrometers. Despite this convincing trend in favor of SHPo surface, the widely inconsistent quantitative results in the literature have led to some fundamental misunderstandings and false anticipations, which we intend to remedy first in the next two subsections.

1.4 Apparent contact angle versus effective slip

A SHPo surface is commonly defined as a surface on which water forms a contact angle over 150° (Quéré 2005) and rolls off easily. In contrast, on a smooth surface of any hydrophobic material, the contact angle of water has never been found larger than $\sim 120^\circ$. It is well understood that such a highly water-repelling property can be obtained if a surface is both chemically hydrophobic and physically rough, whether found in nature (Barthlott and Neinhuis 1997) or artificially created (Kim and Kim 2002). Liquid wetting on rough surfaces is commonly elucidated by two classical models—Wenzel model (Wenzel 1936) and Cassie (or Cassie–Baxter) model (Cassie and Baxter 1944). Wenzel model describes the state in which a liquid wets the surface roughness to form a solid–liquid homogeneous interface, while Cassie model describes the state in which a liquid wets only the top surfaces of the roughness to form a heterogeneous interface of solid–liquid and gas–liquid. In Wenzel model, the apparent contact angle is given by $\cos \theta_{\text{apparent}} = r \cos \theta$, where r is the ratio of the actual liquid–solid contact area to the projected area and θ is the intrinsic contact angle on a smooth surface. According to the Wenzel model, roughness ($r > 1$) amplifies surface wettability; that is, roughness makes a hydrophilic surface appear more hydrophilic and a hydrophobic surface more hydrophobic. In Cassie model, on the other hand, the apparent contact angle is expressed as $\cos \theta_{\text{apparent}} = \phi_s \cos \theta - \phi_g$, where ϕ_s is the ratio of the

¹ We use SHPo instead of the more common SHP or SH to avoid confusion with superhydrophilic (SHPi), which is important for other related disciplines (e.g., coating, heat transfer, optics). Furthermore, the H in SHPo and SHPi are kept (instead of the shorter SPo or SPi) to differentiate them from the likes of superlyophobic, superoleophobic, and superomniphobic (Liu and Kim 2015).

liquid–solid contact area to the projected area (i.e., solid fraction) and ϕ_g is the ratio of the liquid–gas interfacial area to the projected area (i.e., gas fraction).² For the Cassie model, roughness always increases the apparent contact angle; that is, roughness makes any surface appear less hydrophilic (i.e., more hydrophobic).

Although both Wenzel and Cassie models predict that the apparent contact angle becomes larger than the intrinsic contact angle if a hydrophobic surface is roughened, the slippage effects expected from the two models are significantly different. The Cassie state (or partially wetted state) can provide a significant slip effect because of the gas in between surface structures. The much lower viscosity of a gas compared to a liquid (typically by 2–3 orders of magnitude, e.g., the water-to-air ratio of ~ 50 , at room temperature) gives rise to the effective slip even under the conventional no-slip assumption. In comparison, the Wenzel state, with the liquid in between the structures, would provide a negligibly small effective slip despite the large apparent contact angle. To have a large effective slip, not only a SHPo surface (e.g., rough and hydrophobic surface) is needed but also its wetting state should be SHPo (i.e., Cassie state) during the flows. However, it should be further understood that the SHPo state is merely a necessary condition for an effective slip, as explained next.

1.5 Large contact angle does not mean a large slip

We are compelled to emphasize that the apparent contact angle, which is the most common property used to characterize a SHPo surface, should not be construed as the measure of liquid slip or drag reduction. It is unfortunate that numerous publications on SHPo surfaces casually claim their utilities for drag reduction simply because they exhibit a large contact angle. For example, on a certain surface structure, water in Cassie state may have an apparent contact angle nearly 180° but only a negligibly small slippage. As a matter of fact, as discussed in the previous section, even water in a Wenzel state (i.e., negligible slip) may have an apparent contact angle over 150° .

In this review, we will establish that the contact angle, which can be easily measured and readily calculated by the solid fraction on a Cassie surface, is simply one of the

parameters that affect the amount of slip. Fortunately, the recent advances in the field have made it possible to quantitatively predict the slip length from the geometry of the surface structures, as summarized in Sect. 2. Once known, the slip length can predict the amount of drag reduction in a laminar flow system based on the flow geometry of the system, as summarized in Sect. 1.2.

1.6 The motivation of the critical review

To obtain slip lengths sufficiently large for a target application, we have to firstly understand what factors determine the slip length on SHPo surfaces. However, the numerous experimental studies in the literature have reported (many erroneously, as discussed in Sects. 3.2.5 and 3.3.5) a wide range of slip lengths spanning from tens of nanometers to even millimeters on SHPo surfaces consisting of regular (periodic) structures (Ou et al. 2004; Ou and Rothstein 2005; Choi et al. 2006; Davies et al. 2006; Truesdell et al. 2006; Maynes et al. 2007; Steinberger et al. 2007; Byun et al. 2008; Lee et al. 2008; Tsai et al. 2009; Jung and Bhushan 2010; Lee and Kim 2011a; Kashaninejad et al. 2012; Kim and Hidrovo 2012; Maali et al. 2012; Karatay et al. 2013; Bolognesi et al. 2014; Lee and Kim 2014) or random structures (Watanabe et al. 1999, 2003; Gogte et al. 2005; Choi and Kim 2006a; Joseph et al. 2006; Bhushan et al. 2009; Govardhan et al. 2009; Shirtcliffe et al. 2009; Wang et al. 2009; Kim and Hwang 2010; Li et al. 2010; Wang and Bhushan 2010; Ming et al. 2011; Lee et al. 2012; Srinivasan et al. 2013). Sometimes orders-of-magnitude differences in the measured slip lengths were reported even on structurally similar SHPo surfaces (e.g., Lee et al. 2008 vs. Truesdell et al. 2006), testifying the difficulty to accurately measure the slip lengths.

The large disparities in slip lengths among different studies made it difficult to fully understand the relationship between the surface features of SHPo surfaces and the slip length. Following early work (Philip 1972a, b), many analytical models about slip lengths on simple SHPo surfaces have been developed (Lauga and Stone 2003; Ybert et al. 2007; Sbragaglia and Prosperetti 2007a, b; Davis and Lauga 2009a, b; Feuillebois et al. 2009; Belyaev and Vinogradova 2010a, b; Davis and Lauga 2010; Asmolov and Vinogradova 2012; Cottin-Bizonne et al. 2012) and corroborated by numerical simulations (Cottin-Bizonne et al. 2003, 2004; Priezjev et al. 2005; Hendy and Lund 2007; Biben and Joly 2008; Hyvalouma and Harting 2008; Teo and Khoo 2008; Cheng et al. 2009; Ng and Wang 2009, 2010; Teo and Khoo 2010). By fabricating near-perfect microstructures in an extremely clean condition, Lee et al. (2008) succeeded to measure the slip length as a function of surface features, finally verifying the early theoretical models (Lauga and Stone 2003; Ybert et al. 2007) quantitatively and bringing a conclusion to the issue.

² Often considered is a roughness truncated on top with the liquid contacting only the top surfaces and the liquid–gas interface staying flat and in line with the top surfaces. In this simple case (i.e., both the liquid–gas and liquid–solid interfaces in flush configuration) commonly found in the literature, including Fig. 1c, the projected area can be divided into a liquid–solid and a liquid–air interface, i.e., $\phi_s + \phi_g = 1$, so that the Cassie–Baxter equation becomes $\cos \theta_{\text{apparent}} = \phi_s \cos \theta - (1 - \phi_s)$ or $\cos \theta_{\text{apparent}} = (1 - \phi_g) \cos \theta - \phi_g$.

Today we understand how SHPo surfaces would reduce the drag of liquid flows much better than the early 2000s, prompting us to look back and put together the community's achievement in a coherent manner at least for laminar flows. As the slip length on a given SHPo surface and the resulting drag reduction in a laminar flow system are now quantitatively predictable, in this review we apply the available analytical predictions to the laminar experimental data in the literature and discuss why the measured slip lengths scattered so much in early years. Despite the advancement in knowledge, however, so far no drag reduction has been reported in realistic flow conditions. Since the main culprit is the deterioration of the entrapped gas layer on the structured surfaces fully immersed in water (called "plastron" by many today), at the end we discuss the recent efforts to bring about SHPo surfaces that can maintain the plastron. This review aims to help readers predict the slip length of SHPo surfaces and design own SHPo surfaces for their flow applications.

2 Liquid slips on SHPo surfaces: theoretical predictions

Analytical models and numerical simulations are useful tools in understanding slip lengths in laminar flows on a few simple surface patterns such as grates (ridges, trenches) (Philip 1972a, b; Lauga and Stone 2003; Belyaev and Vinogradova 2010a; Asmolov and Vinogradova 2012), posts (pillars) (Ybert et al. 2007; Davis and Lauga 2010), and holes (Ybert et al. 2007; Davis and Lauga 2009a), as shown in Fig. 2. Also, the heights of the structures are assumed uniform, resembling the truncated roughness shown in Fig. 1c. In these models, generally assumed is there no slip on the liquid–solid contact and shear-free conditions (i.e., an infinite slip length) at the liquid–gas interface. According to these studies, for a given pattern type, the structural pitch (i.e., periodicity of the surface structures) and the gas fraction (or solid fraction) are the two most important parameters in determining slip lengths.

2.1 Influence of structural parameters on slip length

On grates parallel to a liquid flow, the slip length is expressed as a function of the gas fraction and the structural pitch (Philip 1972b; Lauga and Stone 2003):

$$\frac{\delta}{L} = \frac{\ln [\sec (\pi \phi_g / 2)]}{\pi} \quad (1)$$

where L is the structural pitch of a grate pattern (i.e., center-to-center distance between two adjacent grates). On grates transverse to a liquid flow, a slip length is given as

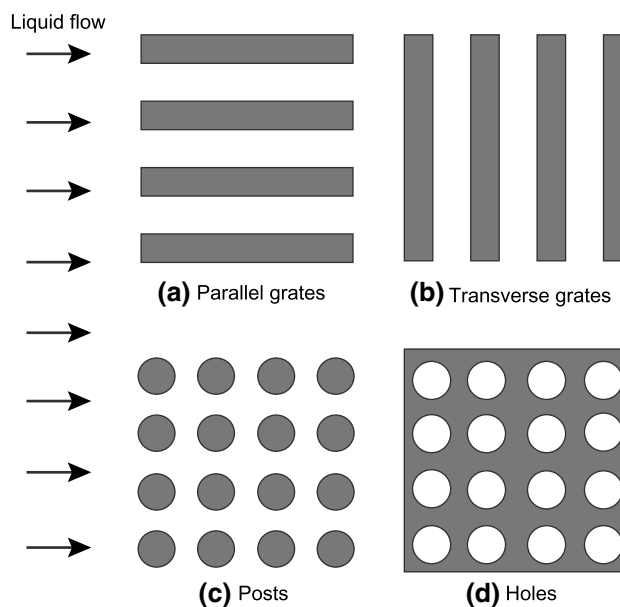


Fig. 2 The simple patterns of the SHPo surfaces modeled for theoretical predictions. **a** Grates parallel to the liquid flow. **b** Grates transverse to the liquid flow. **c** Posts. **d** Holes

a half of that on grates parallel to a liquid flow (Lauga and Stone 2003):

$$\frac{\delta}{L} = \frac{\ln [\sec (\pi \phi_g / 2)]}{2\pi} \quad (2)$$

Analytical solutions for slip lengths on posts were derived for large gas fractions (i.e., $\phi_g > 0.3$) as follows (Davis and Lauga 2010):

$$\frac{\delta}{L} = \frac{3}{16} \sqrt{\frac{\pi}{(1-\phi_g)}} - \frac{3 \ln (1+\sqrt{2})}{2\pi} \quad (3)$$

In case of holes, a logarithmic dependency of slip length on gas fraction was derived analytically (Ybert et al. 2007):

$$\frac{\delta}{L} = -A \ln (1-\phi_g) + B \quad (4)$$

where A and B are prefactors obtained by numerical simulations. For an example, in the case of circular holes at a gas fraction between 0.25 and 0.78, they were obtained as $A = 0.134$ and $B = -0.023$ (Ng and Wang 2010). These analyses assumed the simple Cassie state where $\phi_s + \phi_g = 1$; see the footnote in Sect. 1.4.

The expressions of slip lengths on the simple surface patterns of Fig. 2 predict that slip length depends proportionally on the structural pitch and logarithmically (for grates and holes) or algebraically (for posts) on the gas fraction. As a result, the slip length on posts increases much more steeply at high gas fraction compared to grates and holes.

The different functional expression of slip length on each pattern type can be physically understood using a simple scaling analysis (Ybert et al. 2007). According to the scaling analysis, at a high gas fraction, the average slip velocity is scaled as $u_s \sim U$ and the frictional stress is only applied on the solid area as $\sigma_w \sim \eta(1 - \phi_g)U/a$, where U , η , and a are the far field liquid velocity, liquid viscosity, and the typical size of the solid area, respectively. Then, from the definition of the slip length ($\sigma_w = \eta\dot{\gamma}_w$ and $u_w = \delta\dot{\gamma}_w$, where $\dot{\gamma}_w$ and u_w represent wall shear rate and wall slip velocity, respectively), the effective slip length is given by $\delta \sim a/(1 - \phi_g)$. For grates ($1 - \phi_g = a/L$), this scaling law is simplified to be $\delta \sim L$, while for posts ($1 - \phi_g = (a/L)^2$) it is simplified to be $\delta \sim L/\sqrt{1 - \phi_g}$. Both cases are in good agreement with the exact solutions.

2.2 Secondary influences on slip length

2.2.1 Deviations from the simple conditions

According to the above prediction, the slip length can be considered as a property of a given surface, with the structural pitch and gas (or solid) fraction being the only determinants of slip lengths for a given pattern type. Although invaluable for their ability to guide in the design of SHPo surfaces, the above analyses were based on the assumption of a simple (flush) Cassie state (i.e., $\phi_s + \phi_g = 1$) and a shear-free meniscus. In reality, a SHPo surface may not have a truncated roughness (i.e., flat top surfaces); the liquid–air interface may not stay flat or anchored to the structure top; and the liquid–air interface is not totally shear-free. These deviations further influence the slip length.

A pressure difference between the trapped gas and surrounding liquid would cause the liquid–air interface to deviate from the simple Cassie state, as illustrated in Fig. 3. A deviation from the flush state can be considered as a combination (Fig. 3c) of the displacement (departure) of the menisci from the structure top (Fig. 3a) and the deformation (curving) of the menisci from the flat shape (Fig. 3b). In view of the Cassie states, displacement into the structures means the liquid contacts more than the top surfaces (i.e., $\phi_s > 1 - \phi_g$ even if no deformation), and deformation means the meniscus has a larger area than the flat shape (i.e., $\phi_g > 1 - \phi_s$ even if no displacement).

2.2.2 Meniscus displacement

We will start with the deviation from the flush state by the meniscus displacement as illustrated in Fig. 3a, because it tends to affect the slip length most significantly. Here, displacement means the contact line of the liquid–gas interface is depinned from the top corner of the surface structure and slides away from it. If the meniscus (while assuming flat)

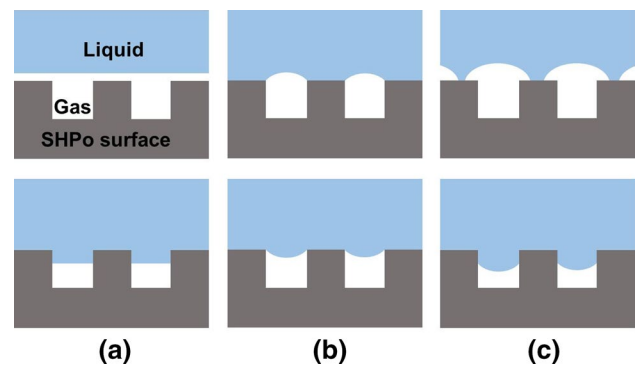


Fig. 3 Possible configurations of the liquid–air interface deviating from the simple Cassie state (i.e., $\phi_s + \phi_g = 1$). **a** Flat meniscus is displaced off the structures (*top*) or into the structures (*bottom*). **b** Meniscus, while pinned at the *top corners* of the structures, deforms away from the structures (*top*) or into the structures (*bottom*). **c** Deformed meniscus is displaced to spread on the structures (*top*) or slide into the structures (*bottom*)

intrudes (penetrates into) the void of the surface structures (Fig. 3a-bottom), the slip length would decrease according to the theoretical studies of (Biben and Joly 2008; Ng and Wang 2009). A numerical study shows that even a very small amount of penetration can lead to a non-negligible amount of decrease in the slip length (Biben and Joly 2008; Teo and Khoo 2010). On the other hand, if the flat meniscus is detached off the surface structures, as shown Fig. 3a-top, a uniform gas layer resembling Fig. 1b will provide a very large (infinite if shear-free interface is assumed) slip length. Although provided here to complete the cases, such a uniform gas layer exists only hypothetically as discussed in Sect. 1.3.

2.2.3 Meniscus deformation

The deviation from the flush state by the meniscus deformation, as illustrated in Fig. 3b, has been analytically tackled in (Sbragaglia and Prosperetti 2007a; Davis and Lauga 2009b; Teo and Khoo 2010), which showed the deformation generally decreases the slip length. When the meniscus is deformed downwardly into the structures (Fig. 3b-bottom) while anchored on top of the structures, it leads to the decrease in slip length (Sbragaglia and Prosperetti 2007a; Davis and Lauga 2009b; Teo and Khoo 2010). However, if the meniscus is deformed upwardly into the liquid while anchored on top of the structures (Fig. 3b-top), the slip length may slightly increase from that of the flush state. According to the analytical model (Davis and Lauga 2009b), the increase peaked at the protrusion angle (i.e., the angle the meniscus forms with respect to the surface) of about 10° . However, if excessive ($>30^\circ$), the upward deformation drastically decreases the slip length, and for the protrusion angle larger than 60° the slip length becomes

even negative (i.e., the frictional drag larger than that on the smooth surface) (Davis and Lauga 2009b). An early theoretical study (Richardson 1973) presented a similar argument that even a perfectly slipping interface can lead to a no-slip boundary condition if the interface is corrugated enough (i.e., similar to Fig. 3a-top but with the liquid–gas interface in a sinusoidal shape).

2.2.4 Meniscus displaced and deformed

Figure 3c illustrates the meniscus being both displaced and deformed. Since for Fig. 3a-bottom the meniscus is depinned and pushed downward most likely by the liquid pressure, in reality the meniscus is likely deformed downwards as well, as shown in Fig. 3c-bottom. Adding the effect of downward displacement and downward deformation, this meniscus shape is expected to lead to a decreased slip length compared with the flush condition. On the other hand, if the depinned contact line spreads on the top surface of the structures (Fig. 3c-top) for example due to the shear of the liquid flow as shown in the numerical study of Gao and Feng (2009), the overgrown gas pockets may enhance the slip. In addition, the neighboring gas pockets may merge to form larger pockets and further increase the slip, the hypothetical case of Fig. 3a-top being the ultimate. While this merged gas pockets will provide a very large slip length when present, they are unstable and expected to exist only temporarily. These overgrown gas layers are more common on irregular structures, which will be addressed in Sect. 3.3.

2.2.5 Meniscus with finite slip

For the deviation from a shear-free meniscus, i.e., the effect of a finite dissipation at the liquid–gas interface, Ybert et al. (2007) reported that the modified slip length δ_{modified} can be generally expressed using the following heuristic formula

$$\frac{1}{\delta_{\text{modified}}} = \frac{1}{\phi_g \delta_{\text{gas}}} + \frac{1}{\delta} \quad (5)$$

where δ_{gas} is the slip length at the uniform liquid–gas interface with no meniscus displacement or deformation but only considering the finite viscosity effect of the gas, and δ is the predicted slip length from Eqs. (1–4). When the gas flows with the liquid in the same direction, δ_{gas} can be estimated based on the shear stress balance at the liquid–gas interface such as $\delta_{\text{gas}} = h(\eta_{\text{liquid}}/\eta_{\text{gas}} - 1)$, where η_{liquid} and η_{gas} are the viscosities of liquid and gas, respectively, and h is the thickness of a gas layer. A similar formula has also been proposed by Hendy and Lund (2007), and its prediction has been shown to agree well with the numerical results for grates. Specifically, the analytical solution on grates has been derived by Vinogradova and co-workers

(Asmolov and Vinogradova 2012; Belyaev and Vinogradova 2010a, b; Vinogradova and Belyaev 2011). For flows parallel to the grates, the modified slip length is given by the following equation.

$$\delta_{\text{modified}} = \frac{L}{\pi} \frac{\ln[\sec(\pi \phi_g/2)]}{1 + \frac{L}{\pi \delta_{\text{gas}}} \ln[\sec(\pi \phi_g/2) + \tan(\pi \phi_g/2)]} \quad (6)$$

For flows transverse to the grates, the modified slip length can be predicted by the following equation.

$$\delta_{\text{modified}} = \frac{L}{2\pi} \frac{\ln[\sec(\pi \phi_g/2)]}{1 + \frac{L}{2\pi \delta_{\text{gas}}} \ln[\sec(\pi \phi_g/2) + \tan(\pi \phi_g/2)]} \quad (7)$$

Not surprisingly, all of the above equations predict the slip length will decrease if the liquid–gas interface is not shear free.

The above analyses assumed the lubricating gas flows with the liquid in the same direction. However, in most cases the gas should be kept on the SHPo surface as a plastron. As the liquid flows over the surface, the trapped gas would circulate inside the tight space between the liquid and the substrate, entailing a viscous friction larger than the above predictions (i.e., smaller δ_{gas}). This further deviation from the shear-free meniscus assumption was later investigated theoretically by Busse et al. (2013). The effect of the confined gas on the overall slip length was introduced into the analytical model for flows transverse to the grates by Nizkaya et al. (2014).

2.2.6 Additional influences

In addition to the liquid–gas meniscus, other factors may influence the slip length albeit in a less pronounced way. Reynolds number (Cheng et al. 2009; Hyvalouma and Harting 2008), a confinement condition (the channel height being much smaller than the free surface distance between structures) (Philip 1972a; Sbragaglia and Prosperetti 2007a), and a slip on solid patches (Choi et al. 2006; Cottin-Bizonne et al. 2004; Hendy and Lund 2007; Ybert et al. 2007) can affect slip lengths under certain conditions.

2.2.7 General effect of the secondary influences

As will be discussed in the following sections, some of these secondary influences—especially the displacement of the meniscus—might be a key to understanding the disparity of slip lengths observed in many experimental studies, although it is not easy to quantify their influences in actual experiments. As discussed above, other than a couple of exceptions most of these secondary factors hamper the slippage and reduce the slip lengths.

2.3 Irregular (random) structures: compared with regular structures

Although it is difficult to quantify, several recent theoretical and numerical works have investigated a slip length on irregularly patterned structures (Feuillebois et al. 2009; Vinogradova and Belyaev 2011; Samaha et al. 2011; Cottin-Bizonne et al. 2012). Samaha et al. (2011) showed that randomly arranged posts render a slightly more slippage than regularly arranged posts of the same solid fraction. However, the random posts exhibited lower stability against the wetting transition, leading to the smaller slip lengths at a given liquid pressure. Cottin-Bizonne et al. (2012) studied the slip length on one-dimensional and two-dimensional fractal structures (i.e., uniform height) both analytically and numerically, and demonstrated that hierarchical fractal structures always underperformed in terms of the slip length compared with single-scale post structures of the same gas fraction. Also, unlike post structures, the slip length does not increase divergently on hierarchical fractal structures even at an infinitely high gas fraction. Note, however, hierarchical fractal structures are likely to outperform when it comes to the plastron stability. Theoretical studies of irregular structures have been limited to the structures of a uniform height (i.e., truncated on top), while in reality the irregularity in the structure height plays a much more important role, as will be discussed in Sect. 3.3.

3 Liquid slips on SHPo surfaces: experiments

3.1 Measurement techniques of slip length

In measuring slip lengths on SHPo surfaces, several different experimental techniques have been employed, many of which were similar to those used in a slip study on smooth surfaces (Neto et al. 2005). Figure 4 lists the measurement techniques used in the experimental studies. The slip measurement approach can be largely classified into direct methods and indirect methods. In the case of direct methods, the slip length is obtained from a velocity profile optically probed on a SHPo surface. In indirect methods, the slip length is estimated from other measurable properties, such as the flow rate or shear stress, which are affected by the slip.

In an indirect way, one can investigate the slip from the relationship between pressure drop and flow rate across a channel whose inner surfaces are at least partially SHPo, as shown in Fig. 4a. The slip length can be deduced from the flow rate increase or pressure drop decrease by the slip (Watanabe et al. 1999; Ou et al. 2004; Choi et al. 2006; Jung and Bhushan 2010; Shirtcliffe et al. 2009; Kim and Hwang 2010; Kashaninejad et al. 2012; Kim and Hidrovo

2012; Lee and Kim 2014). For example, in a microchannel with a circular cross section, the volume flow rate Q driven by the pressure gradient dP/dx can be expressed as a function of slip length δ as shown in the following equation.

$$Q = -\frac{\pi r^4}{8\eta} \frac{dP}{dx} \left(1 + \frac{4\delta}{r}\right) \quad (8)$$

where r is the channel radius and η is a liquid viscosity. While this approach is simple in principle, its implementation is limited by the liquid intruding the microstructures even at a relatively small pressure (e.g., 1 kPa) or by small bubbles trapped inside the hydrophobic channels. Although the liquid intrusion into the surface structures reduces the slip length as reported in Sect. 2.2, additional liquid passage created by the intruded liquid might increase the flow rate through microchannel, leading to the overestimation of the slippage effect (Kim and Hidrovo 2012; Lee and Kim 2014). Also, the effective liquid viscosity might undergo a slight change during measurement depending on the solubility of gas in water (Westin et al. 2003). Lastly, it is not always easy to estimate the actual channel geometry when the SHPo structures are directly generated inside the channel or the channel experiences a deformation when the microchannel is not sufficiently rigid.

As shown in Fig. 4b, micro-particle image velocimetry (micro-PIV) has been widely used as a direct way to measure a velocity profile close to the wall and extract a slip length from the measured velocity profile (Gogte et al. 2005; Ou and Rothstein 2005; Joseph et al. 2006; Byun et al. 2008; Tsai et al. 2009; Karatay et al. 2013; Bolognesi et al. 2014). In this method, fluorescent particles dispersed in water are used as a tracer for the liquid velocity. It has advantages over other methods in that it not only detects a slip length in a direct way but also provides detailed spatial information of the slip on SHPo surfaces, where the interfacial boundaries are intrinsically heterogeneous. Micro-PIV is known to measure a slip length with an accuracy of 100 nm at best, as its accuracy is limited by the determination of the wall location and the interaction of particles with the wall (Joseph and Tabeling 2005). While a direct way to measure the slip length, PIV is not a direct way if one wants to obtain the drag of a flow, for which shear force reading is an example of a direct method.

Another indirect approach to slip measurement is to measure shear stress or frictional drag on a SHPo surface (Choi and Kim 2006a; Truesdell et al. 2006; Steinberger et al. 2007; Lee et al. 2008; Bhushan et al. 2009; Govardhan et al. 2009; Wang et al. 2009; Li et al. 2010; Lee and Kim 2011a; Ming et al. 2011; Lee et al. 2012; Maali et al. 2012; Srinivasan et al. 2013). Despite its relatively low accuracy ($>1 \mu\text{m}$ in measurable slip length), the commercial rheometer has shown to be a convenient tool when measuring a

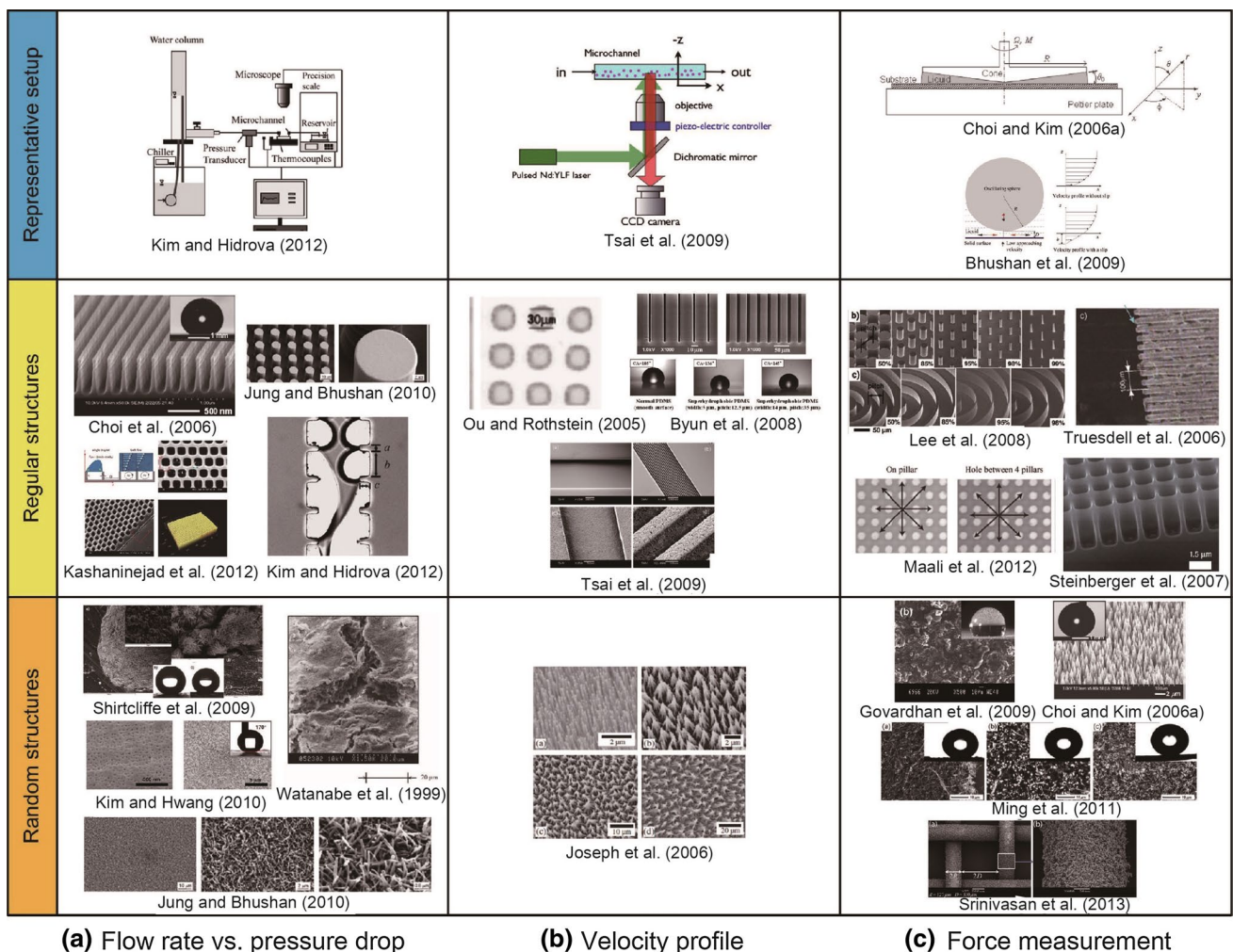


Fig. 4 Experimental techniques used for the slip measurements and surface structures (both regular and random structures) probed by each measurement technique

large slip length (e.g., $>5 \mu\text{m}$), as shown in Fig. 4c (Choi and Kim 2006a; Truesdell et al. 2006; Lee et al. 2008; Li et al. 2010; Ming et al. 2011; Lee and Kim 2011a; Lee et al. 2012; Srinivasan et al. 2013). Not being pressure-driven, the typical surface structures are not intruded by the liquid. In a rheometry measurement, the liquid is squeezed between a cone (or a plate) and a SHPo surface, and is sheared by a rotating cone. Then, the resultant torque is used to estimate a slip length. In this cone and plate configuration, the relationship between the torque and slip length is given by the following equation (Lee et al. 2008).

$$M = \frac{2\pi\eta\Omega R^3}{3\theta_0} \left[1 - \frac{3\delta}{2R\theta_0} + \frac{3\delta^2}{R^2\theta_0^2} - \frac{3\delta^3}{R^3\theta_0^3} \ln \left(\frac{R\theta_0 + \delta}{\delta} \right) \right] \quad (9)$$

where θ_0 , Ω , and R are cone angle, applied angular velocity, and cone radius, respectively. For accurate measurement of slip lengths using rheometry, the influence of liquid–gas

meniscus along the outer edge of the cone or plate should be taken into proper consideration (Bocquet et al. 2006; Choi and Kim 2006b; Lee et al. 2008). Different wettability of the tested surfaces can induce different effective liquid–solid contact line and liquid–gas meniscus shape at the cone edge as well as the effective liquid volume to be sheared. One way to minimize this effect is forming a trench ring or a hydrophilic patch at the location of the cone edge on the sample surface and pinning the contact line of the meniscus there (Lee et al. 2008; Srinivasan et al. 2013).

Also, a custom-built strain gauge can be used to measure the shear stress applied on SHPo surface. A strain gauge has been incorporated into microfluidic channel to measure shear stress at a given flow rate (Govardhan et al. 2009). A better precision can be obtained with atomic force microscopy (AFM) (Bhushan et al. 2009; Wang et al. 2009; Maali et al. 2012) or surface force apparatus (SFA) (Steinberger et al. 2007), which were initially applied to

measure the nanometric slips on a smooth surface (Neto et al. 2005). In AFM, a drainage force is measured when a sphere is approaching the SHPo surface, and a slip length is estimated by comparing the measured force to the theoretical model (Fig. 4c). In SFA, a force response of a sphere vibrating close to a surface can be used to measure the slip length (Steinberger et al. 2007). AFM and SFA have the limitation for slip measurement on anisotropic surface structures, and the confinement effect on the slip lengths might become non-negligible with the gap between the probe and surface being comparable to the length scale of the SHPo surfaces.

Proper choice of measurement techniques is crucial for accurate quantification of slip lengths. Also, the accuracy of each measurement system should be taken into proper consideration in measuring slip lengths. The experimental accuracy might be roughly estimated by measuring the slip length on a nonslip surface such as a clean hydrophilic surface.

3.2 Slip measured on regularly structured SHPo surfaces

3.2.1 Collection of slip length data

Many experimental studies have been conducted on regularly structured (e.g., Fig. 2) hydrophobic surfaces, which were usually fabricated by photolithography or molded from a lithographically patterned master. Well-defined structural features on regular structures make the comparison between experimental data and the theoretical predictions easier, helping to establish the correlation between structural features and slip lengths. The experimentally tested regular structures were of simple patterns such as grates (either parallel or transverse to liquid flow) (Ou et al. 2004; Ou and Rothstein 2005; Choi et al. 2006; Davies et al. 2006; Truesdell et al. 2006; Maynes et al. 2007; Byun et al. 2008; Lee et al. 2008; Tsai et al. 2009), posts (Ou et al. 2004; Ou and Rothstein 2005; Lee et al. 2008; Jung and Bhushan 2010; Lee and Kim 2011a; Kim and Hidrovo 2012; Maali et al. 2012; Lee and Kim 2014) and holes (Steinberger et al. 2007; Kashaninejad et al. 2012) as collected in Fig. 5. Only laminar flow experiments have been collected to follow the topic of this review. The experimental data have been roughly converted to the slip length, if not reported directly, using their flow experimental conditions, when possible to do so. In Fig. 5a, the slip length is presented as a function of the structural pitch to compare with the predicted trend that the slip length should be proportional to the structural pitch, i.e., $\delta \propto L$. In Fig. 5b, the non-dimensionalized slip length (δ/L) is presented as a

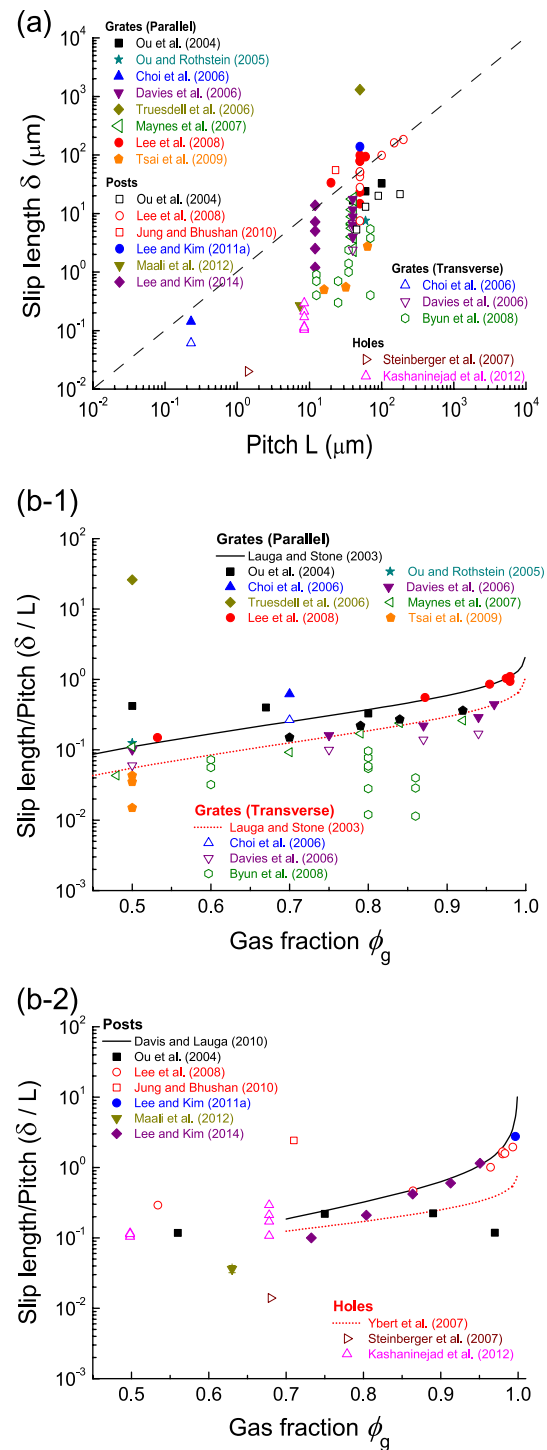


Fig. 5 Measured slip lengths on SHPo surfaces with simple regular patterns. **a** Slip length as a function of the structural pitch. The broken line indicates the general trend of slip length \sim pitch. Most of the data lie below the line. **b** Non-dimensionalized slip length (δ/L) as a function of gas fraction ϕ_g . Lines represent the theoretical predictions (Eqs. 1–4). **b-1** Slip lengths on grates parallel and transverse to the liquid flow. **b-2** Slip lengths on posts and holes

function of the gas fraction along with theoretical predictions for each pattern type. The measured slip lengths on parallel or transverse grates are plotted in Fig. 5b-1, and those on posts and holes are in Fig. 5b-2. Since the graphs had to be drawn on a log–log scale to accommodate all the widely spread data in the literature (except Kim and Hidrovo 2012), note the data reporting large slip lengths deviate more in reality than how they appear in the first sight.

3.2.2 Flow rate versus pressure drop

Flow rate *versus* pressure drop in the microchannels was used for slip measurement in several studies. Ou et al. (2004) reported effective slip lengths up to tens of micrometers on microgrates and microposts and found that the slip length increased with air fraction of the surface structures. In these studies, they fixed the grate width and the post diameter and increased their pitch (periodicity) to increase the gas fraction; the structural pitch and gas fraction varied concurrently. To compare with the theoretical prediction (the lines in Fig. 5b), we isolated the effect of the structural pitch from that of the gas fraction based on the geometric information available. On grates, the measured slip length agreed with the theoretical values at air fraction of 0.8 but overperformed at lower air fractions. On posts, on the other hand, the measured slip length agreed with the theoretical values at the air fraction of 0.75 but underperformed significantly at higher air fractions, perhaps due to liquid intrusion. They also verified that the amount of drag reduction decreased when the channel height (i.e., the characteristic length scale) increased, as theoretically predicted in Sect. 1.2.

Choi et al. (2006) investigated the effect of directionality of grates on liquid slip. Designed mainly to sustain a large liquid pressure (more than 1 atm), the nanometer-scale pitch produced slip lengths below a micrometer, agreeing with the theoretical prediction. Slip lengths of 143 and 61 nm were reported when the grates were parallel and transverse, respectively, to the liquid flow. This ratio was consistent with the 2:1 ratio theoretically predicted by Lauga and Stone (2003). Interestingly, their measured slip lengths were somewhat larger than the theoretical values. It was conjectured that the intrinsic slip on the hydrophobic top surfaces of the grates (tens of nanometers) is not negligible compared with the nanometer-scale structural pitch and slip length, thus contributing to the overall slip.

Jung and Bhushan (2010) tested the SHPo surfaces with various length scales—microposts, nanostructures, and hierarchical structures. For the surface with a regular pattern—microposts, their results showed a large deviation from the theoretical prediction. Moreover, they reported more than 20 μm slip length on smooth hydrophobic

surfaces, raising questions about the validity. The large discrepancy might be attributed to the additional flow due to the channel expansion during the pressure-driven flows.

Kim and Hidrovo (2012) characterized the friction reduction in the microchannel patterned with grates transverse to the liquid flow and correlated it with the wetting state on the surfaces. Interestingly, they demonstrated that the frictional characteristics on the SHPo surfaces could be best characterized by the no-slip condition at the liquid–air interface, which was attributed to the immobilization of the liquid–air interface due to the contamination or interface geometry.

Kashaninejad et al. (2012) tested the eccentricity effects of microhole arrays on the slip lengths by tracking the location of the advancing liquid front at a given applied pressure. Their measured slip lengths of about 1–3 μm agreed well with the theoretical prediction, and the pronounced effects of microhole eccentricity on the slip lengths was reported on microhole arrays with a higher gas fraction.

Lee and Kim (2014) measured the slip length on post arrays while varying the post diameter at a fixed pitch of 12 μm , and their measured slip length showed a good agreement with the theoretical prediction. They showed that SHPo surface might not be the best surface in enhancing the flow rate in microchannels because the space occupied by microscale features can be used as additional liquid passage instead.

3.2.3 Micro-PIV

To measure the slip lengths directly, micro-PIV has been employed in several studies. Ou and Rothstein (2005) measured the slip velocity on the SHPo surfaces using micro-PIV and correlated them with the pressure drop reduction in the microchannel. Byun et al. (2008) shed light on how a liquid–gas meniscus affects the slip length. Their specially designed microchannel enabled a direct visualization of a liquid–gas meniscus during slip measurement. The measured slip lengths using micro-PIV ranged from 0.4 to 5.4 μm , smaller than the theoretical predictions (1–13 μm), which was explained by a wetting transition (i.e., liquid intrusion) visually observed during the measurement. Tsai et al. (2009) measured slip lengths on PDMS microgrates as well as on porous polyvinylidene fluoride (PVDF) microgrates. The measured range of slip length was between 0.5 and 2.5 μm , and PVDF microgrates exhibited a slightly more slippage than PDMS microgrates. Those slip lengths were smaller than the theoretical prediction. Bending of a liquid–gas meniscus into the gas space and a confinement effect were accounted for their smaller slip lengths.

The influence of a protruding liquid–gas meniscus was investigated using micro-PIV in Karatay et al. (2013). In

agreement with their numerical simulation as well as the theoretical prediction by Davis and Lauga (2009b), their measured slip lengths (1–5 μm) decreased rapidly when the protrusion angle increased beyond 10° .

Probing local slippage on a SHPo surface using micro-PIV, Bolognesi et al. (2014) made a similar observation with Kim and Hidrovo (2012) that there is no slippage on the liquid–gas interface. They suggested that the contamination of the liquid–gas interface by particles or PDMS could be the possible cause for the immobilized liquid–gas interface. Indeed, it was recently demonstrated that the intentional contamination of the liquid–gas interface by a surfactant leads to the immobilized liquid–gas interface (Schäffel et al. (2016)).

3.2.4 Shear stress measurement

Shear stress measurement on SHPo surfaces was used to measure the slip lengths in many studies. Measuring the shear on microgrates of 50 μm pitch and 0.5 air fraction using rheometry, Truesdell et al. (2006) reported a giant slip length reaching 1 mm. Their measurement was corroborated by velocity profile measurement using PIV. The microgrates were formed from PDMS and coated with a thin layer of a SHPo material, creating a hierarchical SHPo structure. Their abnormally large slip was attributed to the secondary SHPo coating (thus gas pockets) on the top surface of the microgrates. However, recent theoretical (Cottin-Bizonne et al. 2012) and experimental (Lee and Kim 2011a) studies about slips on hierarchical structures suggest that an additional slip by the secondary roughness could not be that significant. Overall, the slip length 2–3 orders-of-magnitude larger than the prediction is difficult to explain.

Lee et al. (2008) conducted a systematic study to investigate the influence of two surface parameters (i.e., structural pitch and solid fraction) of microgrates and microposts on slip length using cone-and-plate rheometry. In theory, the slip can be increased as far as the structural pitch or gas fraction increases, but in reality the liquid intrudes into large voids easily, limiting the experimentally obtainable slip. Developing defect-free samples (i.e., no missing or damaged structures) and taking advantage of the low pressure (i.e., 200–300 Pa) in their rheometry setup, they were able to test very large gas fractions (up to 0.98 and 0.99 for grates and posts, respectively, at 50 μm pitch) and very large structural pitches (up to 200 and 60 μm for grates and posts, respectively, at 0.98 gas fraction) before encountering the wetting transition. On grates and posts, slip length increased rapidly with gas fraction and linearly with pitch, showing an excellent agreement with the theoretical predictions (Lauga and Stone 2003; Ybert et al. 2007; Davis and Lauga 2010) (Fig. 5b). Although at the same gas fraction,

posts outperformed grates in terms of slip length, further consideration led to the conclusion that grates are more advantageous for slip lengths over posts due to their higher stability against wetting transition. This study conveyed two important messages about frictional drag reduction using SHPo surfaces. First, a giant slip length more than 100 μm could be obtained only under well-controlled laboratory conditions (e.g., low liquid pressure and no surface defects). Second, it showed that a compromise between a wetting transition and a slippage effect should be considered in designing SHPo surfaces for the drag reduction. Generally, a SHPo surface capable of providing a large slip length (e.g., large pitch and high gas fraction) is more vulnerable to wetting transition.

Measuring the liquid drainage force with SFA on an array of holes, Steinberger et al. (2007) measured much smaller slip lengths than the theoretical values. Through numerical simulation and elasticity measurements, they demonstrated that the protruding bubbles over holes decreased the slip, which was also supported by another analytical and numerical result (Davis and Lauga 2009b) and experimental measurement (Karatay et al. 2013). More interestingly, their work showed a counterintuitive result that the slip length on non-wetted surfaces (20 nm) was actually smaller than that on wetted surfaces (105 nm), demonstrating that a trapped gas on structured surface does not always help reducing the liquid drag. Using a drainage experiment of water with a colloidal probe AFM, Maali et al. (2012) measured the slip lengths on microposts. They showed that the local slip lengths (i.e., 119 nm) on the solid patches were smaller than those (i.e., 356 nm) on the liquid–air interface as expected, and the effective slip length of 268 nm was calculated by considering the relative contribution of local slip lengths to the overall slip length. In this study, the deviation from the theoretical prediction was explained by the curvature effect of the liquid–air meniscus.

3.2.5 Discussion

Most of the experimental data on patterned surfaces showed a qualitative agreement with the analytical prediction, but quantitatively often the measured slip lengths were lower. In experiments using microchannels, the liquid pressure may deform a liquid–air meniscus (Tsai et al. 2009) or partially or completely intrude the liquid into the voids (Byun et al. 2008; Kim and Hidrovo 2012; Karatay et al. 2013), which results in the decrease of liquid slip. Also, the liquid–air interface might become immobilized due to contamination or geometric condition (Kim and Hidrovo 2012; Bolognesi et al. 2014). This meniscus-induced slip decrease is expected to be more pronounced on microstructures with a larger structural pitch and a higher gas fraction. Also, the confined flow condition (i.e., a small channel height

compared with the structural pitch) inside microchannel can contribute to a further decrease in slip length (Maynes et al. 2007; Tsai et al. 2009) under certain conditions, as predicted by analytical analyses (Sbragaglia and Prosperetti 2007a; Feuillebois et al. 2009) and numerical simulation (Cheng et al. 2009). Lastly, the circulation of the entrapped gas within the microstructures may have decreased the slip length in some cases significantly, as explained by Busse et al. (2013). Those additional factors may explain why many reported slip lengths are smaller than predicted.

Although less often, the measured slip lengths were also found larger than the analytical predictions. The relatively higher values may be explained by the possibilities of expansion of flexible microchannels by pressure (Sect. 3.2.2), added liquid passage in the surface structures (Lee and Kim 2014), and the intrinsic slip on the nanometer-scale solid surfaces (Choi et al. 2006), etc. However, the very large discrepancies (e.g., Truesdell et al. 2006) cannot be explained well unless we invoke the possibility of a thick gas layer overgrown on the microstructures as discussed in Sect. 2.2.4.

3.3 Slip measured on randomly structured SHPo surfaces

3.3.1 Collection of slip length data

Many experimental studies used randomly structured hydrophobic surfaces for their ease of fabrication and perceived relevance to practical applications. The experimentally tested random structures were made by a variety of fabrication methods, such as black silicon etching (Choi and Kim 2006a), metal oxidation (Shirtcliffe et al. 2009), growing nanofibers or nanotubes (Joseph et al. 2006; Kim and Hwang 2010; Li et al. 2010; Ming et al. 2011), and particle spray coating (Srinivasan et al. 2013). Despite the clear drag reduction effect on randomly structured SHPo surfaces, the irregularity of surface structures makes it difficult to extract the geometric information such as a gas fraction and a structural pitch—the two geometric data needed for the theoretical prediction of the slip length. Nevertheless, using somewhat liberal approximations we have managed to form a unified landscape of Fig. 6, which covers practically all the laminar flow results in the literature (Watanabe et al. 1999; Gogte et al. 2005; Choi and Kim 2006a; Joseph et al. 2006; Govardhan et al. 2009; Shirtcliffe et al. 2009; Wang et al. 2009; Jung and Bhushan (2010); Kim and Hwang 2010; Li et al. 2010; Ming et al. 2011; Lee et al. 2012; Srinivasan et al. 2013). For comparison with the theoretical predictions, in Fig. 6a we first assess the experimental data against the confirmed trend that the slip length should be proportional to the structural pitch or, for the case of random structures here, to the length scale of

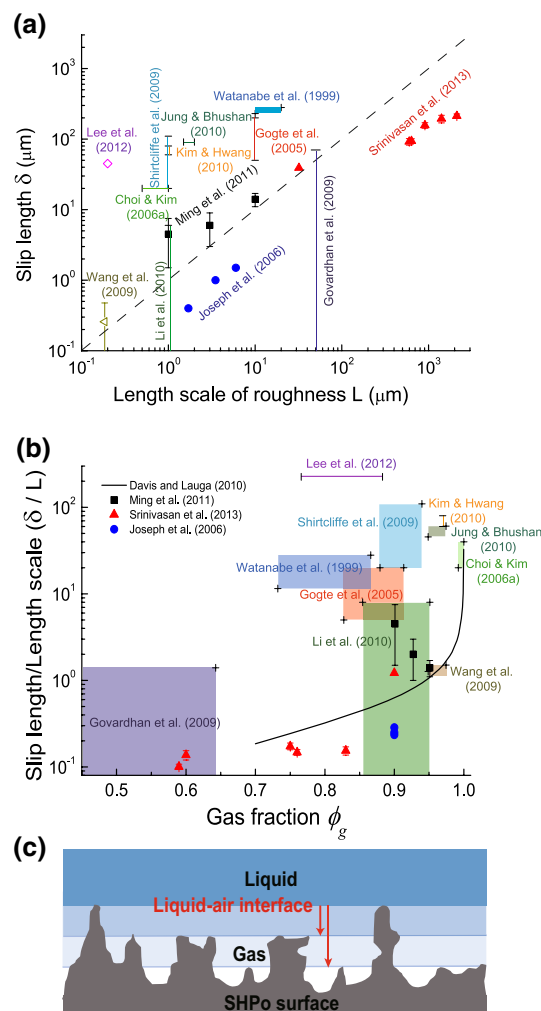


Fig. 6 Estimated or measured slip lengths on SHPo surfaces with random surface structures. **a** Slip length as a function of the length scale of roughness (L). The broken line indicates the general trend of slip length \sim roughness scale. **b** Non-dimensionalized slip length (δ/L) as a function of gas fraction ϕ_g . The black solid line shows the theoretical prediction for posts. The data far off from the dotted line (i.e., $\delta = L$) in (a) or the solid line in (b) suggest a possibility of overgrown plastron, strong secondary effects, or the faulty estimation of the roughness scale or the gas fraction. **c** The schematic illustrates the uncertain nature of liquid–solid contact (i.e., length scale, gas fraction, etc.) on random surface structures. See the discussion in Sect. 3.3.5

roughness, i.e., $\delta \propto L$. Then, in Fig. 6b we compare non-dimensionalized slip length (δ/L) with the prediction for posts as a function of gas fraction.

When the roughness scale and gas fraction were not available, i.e., not mentioned explicitly in the paper, we estimated the roughness scale from the scanning electron microscopy (SEM) images of the surface and the gas fraction from the apparent contact angle θ_{apparent} using the Cassie–Baxter equation $\cos \theta_{\text{apparent}} = (1 - \phi_g) \cos \theta - \phi_g$. When the intrinsic contact angle θ was not available,

we assumed that θ had a value in between 90° and 120° . Deduction of data was needed in some additional cases, too. Many studies on SHPo surfaces with random structures reported their slip lengths, but some reported only the amount of drag reduction (Gogte et al. 2005; Kim and Hwang 2010). Since the drag reduction depends not only on the slip length of the SHPo surface of interest but also on the characteristic length scale of the flow system the SHPo surface is tested in as discussed in Sect. 1.2, we roughly converted the measured drag reductions to slip lengths using the geometric information directly or indirectly reported in each article. Despite all these uncertainties, we decided that the value of the unified graph of Fig. 6 outweighs the possibility of some faulty estimations.

3.3.2 Flow rate versus pressure drop

Many studies measured the enhancement of flow rate at a given pressure drop through a channel with its inner walls coated or modified with a randomly structured SHPo surface. Watanabe et al. (1999, 2003) reported a 14 % drag reduction using a pipe coated with SHPo surfaces, corroborated by a velocity measurement using a hot film anemometer. They reported a larger drag reduction in a pipe with a larger diameter (12 vs. 6 mm), which contradicts directly with the proven prediction of Sect. 1.2. Also, a drag reduction was observed only under laminar flows; no drag reduction was observed when the liquid flow became turbulent.

Shirtcliffe et al. (2009) tested drag reduction using a copper tube whose inside was modified with oxidation and hydrophobic coating, and reported 10–100 μm slip lengths whose magnitude decreased with an increasing flow rate. They attributed the decreasing slip to the weakened stability of the gas layer at large pressures (i.e., high flow rate).

Kim and Hwang (2010) fabricated PTFE tube whose inside was covered with nanofibers and measured 50–65 % faster flow rate across the SHPo tube corresponding to 60–80 μm slip length when converted. However, they attributed the fast flow rate to a low contact angle hysteresis rather than the slippage on the trapped gas. Jung and Bhushan (2010) measured slip lengths on various SHPo surfaces including random nanostructures. They reported a slip length of $\sim 90 \mu\text{m}$ on nanostructures made through self-assembled lotus leaf. However, they also reported more than 20 μm slip length on a smooth surface, which suggests a potential systematic measurement error.

3.3.3 Micro-PIV

Joseph et al. (2006) measured a slip length on carbon nanotube forest, using micro-PIV. Particularly, they varied the structural pitch of nanotube forests systematically and revealed that the slip length increased linearly with a

structural pitch, also in good agreement with the theoretical prediction.

3.3.4 Shear stress measurement

Several studies directly measured a frictional drag or shear stress applied onto SHPo surfaces. Gogte et al. (2005) reported an order of 10 % drag reduction on a hydrofoil coated with a SHPo surface. The amount of drag reduction was shown to decrease with Reynolds number as well. Choi and Kim (2006a) used a commercial rheometer in measuring the slip length on tall and sharp nanoneedles with air fraction close to 1. They reported a 20 μm slip length with water, suggesting that a larger slip length than the length scale of the structural pitch would be possible in the extreme case of the air fraction close to 1, which can also be predicted in Eq. 3. They also showed that slip length increased linearly with a viscosity of test liquids, agreeing with the theoretical prediction of the slip length for a liquid flowing over a solid surface covered with a uniform layer of gas, i.e., $\delta = h(\mu_{\text{liquid}}/\mu_{\text{gas}} - 1)$. Also, Li et al. (2010) measured slip length on carbon nanotube pillars using a similar rheometer system and reported up to 6 μm slip length at a low shear rate with an uncertainty level of $\pm 2 \mu\text{m}$. At a high shear rate, the slippage effect was observed to disappear as a wetting transition occurred. In another study by the same group (Ming et al. 2011), they demonstrated that slip length increased as the distance between adjacent carbon nanotube pillars increased, in agreement with the theoretical prediction.

Lee et al. (2012) measured the slip lengths on nanostructured ZnO surfaces using parallel plate rheometry. Slip lengths of about 45 μm were measured on the ZnO SHPo surfaces, but 20–30 μm slip lengths were also measured on the hydrophobic surfaces, suggesting the possibility of a systematic experimental bias. Srinivasan et al. (2013) measured the slip lengths on dual-textured spray-coated SHPo mesh surfaces using parallel plate rheometry while monitoring the location of the liquid–air interface at a given pressure. The reported slip lengths ranged in between 100 and 200 μm , which were comparable to the mesh spacing. Govardhan et al. (2009) measured the flow rate while monitoring the shear stress applied to the wall and reported a higher flow rate on SHPo surface than on a hydrophilic surface at the same applied shear stress. The maximum slip length in their study was about 50 μm , similar to the length scale of roughness on the SHPo surface. They also found that a slip length decreased exponentially over time with a characteristic time of $\sim 1 \text{ h}$. They attributed the decrease of a slip length to a gradual loss of the gas on the SHPo surface. Recently, Bhushan and his colleagues (Bhushan et al. 2009; Wang et al. 2010; Wang and Bhushan 2010) used AFM to measure the slip length on hydrophilic, hydrophobic, and

SHPo surface, and reported about 250 nm slip length on SHPo surfaces, which is comparable to the length scale of their roughness.

3.3.5 Discussion

The results with regular arrays of posts (Fig. 5b-2)—well established both theoretically (Davis and Lauga 2010) and experimentally (Lee et al. 2008)—teaches us that the slip length would be smaller than the structural pitch and become comparable to it, i.e., $\delta/L \sim 1$, only at large gas fraction (e.g., $\delta > 0.9$). Although proven for regular structures, it is highly likely that the same trend applies to random structures. However, the results with random structures (Fig. 6a, b) show that many of the reported data lie way above the reference (broken) line $\delta = L$ (Fig. 6a) or the predicted slip length for posts (Fig. 6b). These results can be partly attributed to the possibility of an overgrown plastron, for which a liquid contacts only taller structures on random SHPo surface, as illustrated in Fig. 6c, making the effective pitch much larger than the estimated from SEM images. However, the very large pitch of such an overgrown plastron would be only temporary as the liquid pressure will soon increase the contact areas (i.e., reduces gas fraction) and reduce the roughness length (i.e., pitch) to balance the pressure. This trend of deteriorating drag reduction over time or at high flow speeds is consistently reported throughout all the experiments using randomly structured surfaces.

When there is a very large discrepancy between the experimental data and theoretical prediction, a systematic error or bias is suspected in the experiments, particularly when an appreciable liquid slippage effect is also measured on smooth surfaces (Jung and Bhushan 2010; Lee et al. 2012). In the case of slip measurements using a microchannel lined with random structures, it would be difficult to precisely determine the internal diameter or height of the channel due to the irregular nature of the surface structures. Furthermore, deformation of the channel assembly under the liquid pressure would affect the measurement of flow rates. Even a slight deformation may influence the slip length value because of the small scale of the setup and small flow rate. In the case of slip measurement using commercial rheometry, caution should be taken to minimize the measurement errors associated with the rheometry system, as discussed in Bocquet et al. (2006) and Choi and Kim (2006b).

3.3.6 Other effects

A few experimental studies (Watanabe et al. 1999; Choi and Kim 2006a) have observed liquid viscosities influencing the slip lengths on random structures. This result is intriguing because such viscosity effect was expected to be

marginal according to the theoretical prediction. Since the heights of random structures are not uniform, unlike regular structures, the actual contact area and structural pitch between the liquid and the SHPo surface might be related to the liquid viscosity (Fig. 6c). Choi and Kim (2006a) attributed the linear relationship between liquid viscosity and slip length to the dissipation at the liquid–gas interface using a simple gas cushion model, assuming the gas fraction on their nanoneedles is close to 1. However, a simple gas cushion model would not be applicable if the gas fraction was moderate, according to the recent analytical studies (Belyaev and Vinogradova 2010a, b; Vinogradova and Belyaev 2011; Asmolov and Vinogradova 2012).

Also, several studies (Watanabe et al. 1999; Gogte et al. 2005) have observed the shear rate (or Reynolds number) and liquid pressure influencing the slip lengths on random structures, similar to the case of regular structures. Normally, slip length was shown to decrease as shear rate or liquid pressure increased. This dependency might be attributed to the increased probability of wetting transition on random structures at higher shear rate and liquid pressure, as schematically illustrated in Fig. 6c. Several studies dedicated to wetting transition on SHPo surfaces showed that there is indeed an increased loss of gas from SHPo surface at high shear rates (Sakai et al. 2010) and liquid pressure (Poetes et al. 2010).

4 What is preventing the success? Vanishing plastron

The unmistakably large slippages found on many SHPo surfaces in recent years have raised the expectation that they may finally bring about a useful drag reduction in field applications, e.g., marine transportation. Unfortunately, no such success has been reported yet, for several reasons. Leaving the manufacturing of functional SHPo surfaces and the economy of implementing them to the future, here we are obligated to discuss a disheartening reality: the SHPo surfaces will lose its trapped gas, i.e., the plastron, in most realistic conditions. The unavoidable nature of the vanishing plastron is presented and the efforts to combat the problem are listed.

4.1 Frailty of plastron on large-slip SHPo surfaces

To realize its true potential, such as an appreciable drag reduction for large-scale fluidic systems (e.g., boats), one needs a SHPo surface that is capable of not only providing a large enough slip but also maintaining the plastron during the service. Following the discussion in Sect. 1.2, we expect a slip length on the order of 10–100 μm for a SHPo surface to be useful for most macroscale applications,

considering the typical boundary layer thickness is in the order of a millimeter. The preceding sections summarized the recent advances found in literature, which now teach us how to design a large-slip SHPo surface reasonably well. As a rule of thumb, a structural pitch comparable to the desired slip length is required, which implies microscale (not nanoscale) structures, whether regular or random, are needed for the slip length in the range of 10–100 μm .

The underlying assumption for all the above predictions was that the plastron exists throughout the usage. However, under water the SHPo surface may lose the plastron via various mechanisms such as gas dissolution and meniscus disruption. When the gas is lost and replaced by the liquid, the effective slip vanishes altogether. Unfortunately, the surfaces that produce larger slips (i.e., large pitch, large air fraction) are more susceptible to the wetting transition, as explained in the previous section. A recent study demonstrated that SHPo surfaces with a useful slip length (i.e., $\sim 100 \mu\text{m}$) cannot maintain the plastron if placed under water deeper than several centimeters even if the environment is made perfectly stable (Xu et al. 2014), confirming the theories formed for such an ideal environment. In contrast, under a usual laboratory environment with temperature and pressure fluctuating, reliable data were not even attainable, explaining why all other stability experiments were only statistical studies. Note almost all the experiments of SHPo surfaces in literature have been performed in an ambient environment with minimized liquid pressure for a short period of time. Also note that the water in most water channel experiments is saturated or even supersaturated with air in the test section where the liquid pressure is often below the atmospheric pressure, sustaining the plastron in a manner not representing the reality outside the laboratory. Things would be much more challenging in most of the important real-life applications, where the surface is fully immersed at a certain depth in the water and moves at high speed for a long period of time. In this section, we will discuss how some recent studies have started to address the issue of vanishing plastron.

The design approach to help keeping the plastron on a SHPo surface includes making the surface resistant to a wetting transition (Carlborg et al. 2008; Lee and Kim 2009; Barthlott et al. 2010; Carlborg and van der Wijngaart 2011) and adding a built-in mechanism that replenishes the gas on the surface on demand (Lee and Kim 2011b, 2012; Lee and Yong 2015). The approach can be categorized depending on whether or not external energy is used, i.e., passive versus active approach, as summarized in Fig. 7.

4.2 Toward robust plastron: passive approach

There have been significant efforts to make the SHPo surface more robust against wetting. Many have reported persistent plastron on natural and artificial SHPo surfaces made with nanoscale structures. Since gas pockets in nanoscale cavities are several orders of magnitude more stable than in microscale cavities, they can stay indefinitely at even a relatively high liquid pressure (e.g., meters of water depth) according to the theoretical predictions proven experimentally by Xu et al. (2014). However, we do not discuss the nanostructured SHPo surfaces here because they do not provide slip lengths large enough to be useful for most engineering applications.

One approach is to make the inner surfaces of the microstructures repel the liquid more strongly. Lee and Kim (2009) generated nanostructures only on the sidewall of silicon microstructures, leaving the top surface smooth (Fig. 7a-1). This modification effectively expanded the maximum obtainable pitch and the gas fraction in the presence of a liquid pressure. Compared with the same SHPo surface with a smooth sidewall, this approach allowed twice the water pressure, which corresponded to an effective contact angle of 180° on the sidewall. Interestingly, they found that the microstructures with nanostructured sidewalls and smooth tops performed better than those with nanostructured sidewalls and nanostructured tops. The latter case is the same as most of the reported hierarchical surfaces, i.e., microstructures covered with nanostructures everywhere. The effectiveness of the more wettable top of otherwise SHPo structures is consistent with the study below.

Another approach is to mimic *Salvinia* leaves (Barthlott et al. 2010). *Salvinia* leaves are covered with hydrophobic hairs each terminating in an eggbeater shape, whose top provides hydrophilic patches on an otherwise SHPo surface (Fig. 7a-2). On these structures, the hydrophilic tips make the water–air meniscus pinned even when the pressure of the trapped air becomes larger than the water pressure (i.e., Figure 3b-top but not Figs. 3c-top or 1a-top), helping preserve the plastron for a long duration even under environmental fluctuation. In the study apparently done at a low water depth, an air layer was shown staying up to 2 weeks on natural *Salvinia* leaves.

To sustain liquid pressure without collapsing the plastron, a side channel was added under the SHPo surface in a way that the air layer on the SHPo surface was automatically compressed by a flowing liquid in the side channel (Carlborg and van der Wijngaart 2011). In this method, a gas layer was compressed between two liquid flows—one in the main channel and the other in the side channel. They

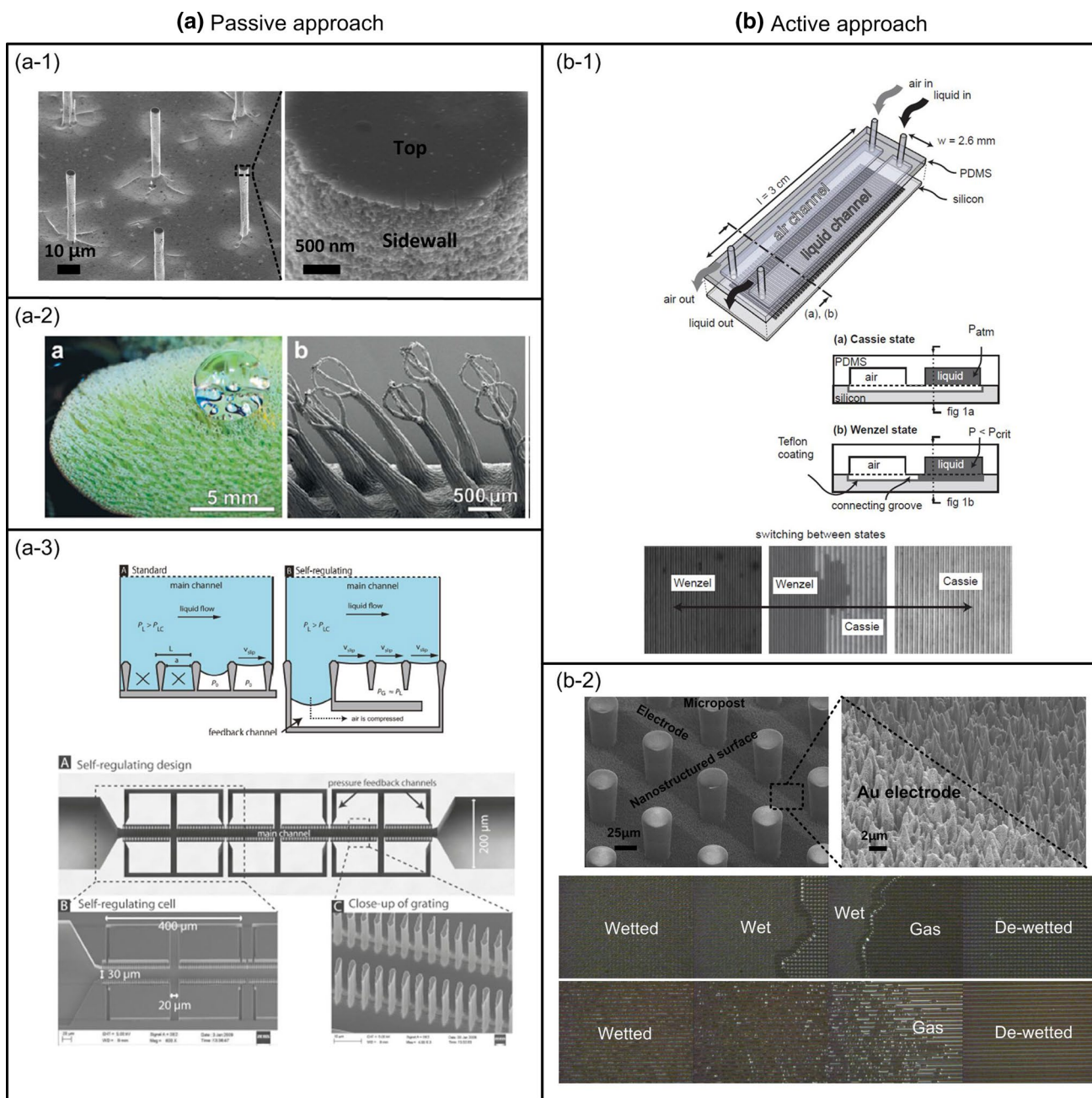


Fig. 7 Reported approaches to address the wetting on SHPo surfaces. **a** Passive approaches **a-1** Nanostructures on the sidewall of microstructures make the SHPo surface more resistant to a wetting transition by the liquid pressure (Lee and Kim 2009); **a-2** Salvinia leaves. Hydrophilic patches at the tip of the surface structures pinned the liquid–air meniscus on the tip, preventing the gas departure from the surface structures (Barthlott et al. 2010); **a-3** self-regulating wetting control. An air layer on SHPo surface is pressurized by the intentional

wetting transition outside the main channel (Carlborg and van der Wijngaart 2011). **b** Active approaches. **b-1** Pressurizing the gas layer using an external tank (Carlborg et al. 2008); **b-2** Replenishing the gas when it is lost from SHPo surface. The combination of two-tier structures (microstructures on the nanostructured bottom) and self-limiting gas generation by electrolysis prevented the wetting even under a very high liquid pressure (7 atm) (Lee and Kim 2011b)

have the same liquid pressure, but one is more vulnerable to the wetting (Fig. 7a-3). As the pressure of the flowing liquid increased, the gas layer became pressurized in a self-regulated manner by triggering an earlier wetting transition

in the side channel, while maintaining non-wetted state in the main channel. This approach increased the maximum sustainable pressure of the SHPo surface from 8 to 25 kPa without any deterioration of slippage effect.

4.3 Toward robust plastron: active approach

The aforementioned passive approaches can be considered preventive measures, as they may prevent or delay the wetting on SHPo surfaces but become ineffectual once the wetting occurs or overwhelmed by a high hydrostatic pressure (e.g., more than 10-m-deep water). From a practical perspective, a more desirable approach would be to restore the plastron when it is lost or compromised, as it would be difficult to deter all the mechanisms that cause the wetting in many different operation conditions.

Related to the passive method, Carlborg et al. (2008) also reported active pressurization of the air layer on SHPo surfaces. In this study, the gas layer was connected to and its pressure controlled by the external tank outside the microchannel (Fig. 7b-1). With this approach, the SHPo state could be sustained up to a water pressure of 60 kPa. However, the pneumatic control with an external source required a priori information of the liquid pressure as well as a complex configuration (e.g., feeding line) and additional bulky component (e.g., air tank).

Lee and Kim (2011b, 2012) have introduced a simple and energy-efficient approach to tackle the wetting problem by automatically restoring the plastron only where and when it is lost on the SHPo surface. They monolithically integrated a self-limiting gas generation mechanism with a hierarchical SHPo surface specifically designed to facilitate the formation of a stable gas film. Their SHPo surface consists of microstructures on top of a nanostructured bottom, on which electrodes are patterned for electrolytic gas generation (Fig. 7b-2). If water intrudes the microstructures, the electrodes generate gas by electrolysis, as the impregnating water closes the electrochemical circuit between the electrode and the conductive liquid. The newly generated gas displaces the wetting liquid out of the surface structures and eventually restores a gas film on the SHPo surfaces. This semi-active method was proven effective under near-realistic conditions, such as a very high liquid pressure (up to 7 atm) and a defective surface. Lee and Yong (2015) also adopted a similar hierarchically structured surface to regenerate a gas layer on SHPo surface. But, they used solar energy instead of electrical energy to initiate the electrochemical gas generation. Please note that vaporizing water might be used to generate a gas layer as well (Vakarelski et al. 2014). However, such thermal vapor would last only while being heated, draining a significant amount of energy.

5 Conclusions and outlook

Through a comprehensive review on the measured slip lengths on various types of SHPo surfaces and their

comparison with theoretical predictions, we showed how SHPo surfaces should be designed for hydrodynamic frictional drag reduction. Geometric features of the surface structures such as pattern type, structural pitch, and gas fraction as well as flow conditions on the surface should be properly considered in designing the SHPo surfaces for effective drag reduction. Particularly, a compromise should be made between how large the liquid slip should be and how robust the plastron should be against wetting, because a SHPo surface for large slip is more susceptible to losing its plastron. Noticing the importance of maintaining the gas layer under the water, a few recent studies reported methods to delay or even prevent the wetting transition.

While the liquid slip and drag reduction for laminar flows are relatively well understood now, the same cannot be said for turbulent flows at this point. The recent numerical (Martell et al. 2009, 2010; Park et al. 2013) and experimental (Daniello et al. 2009) results under turbulent flow conditions have shown that SHPo surfaces with even a moderate slip length ($\sim 10 \mu\text{m}$) can result in significant turbulent drag reduction, as the turbulent structures become weakened near the SHPo surface and a thin viscous sub-layer becomes the main characteristic fluidic length scale in the turbulent flow. Recently, using regular-structured SHPo surfaces of large slip lengths, drag reductions as much as 75 % have been reported in turbulent boundary layer flows (Park et al. 2014). However, an experimental study using a random-structured SHPo surface has reported that at high Re numbers the plastron was found depleted and drag reduction vanished (Aljallis et al. 2013). This trend of deteriorating plastron on random SHPo surfaces was widely seen for laminar flows as well, as discussed in Sect. 3.3 (especially Sect. 3.3.5 and Fig. 6c).

With growing knowledge of the kinds of SHPo surfaces to design and the encouraging initial results for turbulent drag reduction, the time for a field demonstration of turbulent drag reduction seems approaching. However, there are several important issues to be addressed before we see a full deployment of SHPo surfaces in practical applications. A high cost of producing large-area SHPo surfaces is still an obstacle as well as a physical damage or chemical degradation of the SHPo surfaces over time. In particular, biofouling on the surface is a serious issue for underwater vehicles as it incurs additional frictional drag and considerable maintenance effort. Nevertheless, we expect that these issues can be overcome eventually with a rapid development of low-cost micro- and nanofabrication techniques (Ahn and Guo 2009), the development of regenerative SHPo surfaces (Wang et al. 2010), damage-tolerant SHPo surfaces (Lu et al. 2015), rare-oxide-based hydrophobic coatings (Azimi et al. 2013), and the functioning of SHPo surfaces as anti-biofouling surfaces (Genzer and Efimenko 2006).

Lastly, oil-infused nanostructured surfaces (Wong et al. 2011), which have attracted much interest for their liquid repellency as well as their stability under a high liquid pressure, have been hailed as an alternative to the SHPo surface. However, an oil-infused surface can reduce the frictional drag only if the flowing liquid has a significantly larger viscosity than the infused oil (Solomon et al. 2014), excluding water from the candidate pool. Furthermore, the infused oil can be destabilized due to oil depleted under shear (Wexler et al. 2015). Considering these restrictions, despite its great quality for many other applications, we do not expect oil-infused surfaces playing a major role for hydrodynamic drag reductions.

Acknowledgments The work has been partially funded by the ONR Grant No. N000141110503, NSF Grant Nos. 1336966 and 1462499, DARPA Grant HR0011-15-2-0021, KIMM Agreement 20155270, the Alexander von Humboldt Foundation, and NRF-2014R1A1A1002908. The proof reading efforts of Shashank N Gowda, and Muchen Xu are greatly appreciated.

Open Access This article is distributed under the terms of the Creative Commons Attribution 4.0 International License (<http://creativecommons.org/licenses/by/4.0/>), which permits unrestricted use, distribution, and reproduction in any medium, provided you give appropriate credit to the original author(s) and the source, provide a link to the Creative Commons license, and indicate if changes were made.

References

- Ahn SH, Guo LJ (2009) Large-area roll-to-roll and roll-to-plate nanoimprint lithography: a step toward high-throughput application of continuous nanoimprinting. *ACS Nano* 3:2304–2310
- Aljallis E, Sarshar MA, Dala R, Sikka V, Jones A, Choi CH (2013) Experimental study of skin friction drag reduction on superhydrophobic flat plates in high Reynolds number boundary layer flow. *Phys Fluids* 25:025103
- Asmolov ES, Vinogradova OI (2012) Effective slip boundary condition for arbitrary one-dimensional surfaces. *J Fluid Mech* 706:108–117
- Azimi G, Dhiman R, Kwon HM, Paxson AT, Varanasi KK (2013) Hydrophobicity of rare-earth oxide ceramics. *Nat Mater* 12:315–320
- Barthlott W, Neinhuis C (1997) The purity of sacred lotus or escape from contamination in biological surfaces. *Planta* 202:1–8
- Barthlott W, Schimmel T, Wiersch S, Koch K, Brede M, Barczewski M, Walheim S, Weis A, Kaltemaier A, Leder A, Bohn HF (2010) The Salvinia paradox: superhydrophobic surfaces with hydrophilic pins for air retention under water. *Adv Mater* 22:2325–2328
- Belyaev AV, Vinogradova OI (2010a) Effective slip in pressure-driven flow past super-hydrophobic stripes. *J Fluid Mech* 652:489–499
- Belyaev AV, Vinogradova OI (2010b) Hydrodynamic interaction with super-hydrophobic surfaces. *Soft Matter* 6:4563–4570
- Bhushan B, Wang Y, Maali A (2009) Boundary slip study on hydrophilic, hydrophobic, and superhydrophobic surfaces with dynamic atomic force microscopy. *Langmuir* 25:8117–8121
- Biben T, Joly L (2008) Wetting on nanorough surfaces. *Phys Rev Lett* 100:186103
- Bocquet L, Barrat JL (2007) Flow boundary conditions from nano- to micro-scales. *Soft Matter* 3:685–693
- Bocquet L, Tabeling P, Manneville S (2006) Comment on ‘large slip of aqueous liquid flow over a nanoengineered superhydrophobic surface’. *Phys Rev Lett* 97:109601
- Bolognesi G, Cottin-Bizonne C, Pirat C (2014) Evidence of slippage breakdown for a superhydrophobic microchannel. *Phys Fluids* 26:082004
- Busse A, Sandham ND, McHale G, Newton MI (2013) Change in drag, apparent slip and optimum air layer thickness for laminar flow over an idealized superhydrophobic surface. *J Fluid Mech* 727:488–508
- Byun D, Kim J, Ko HS, Park HC (2008) Direct measurement of slip flows in superhydrophobic microchannels with transverse grooves. *Phys Fluids* 20:113601
- Carlborg CF, van der Wijngaart W (2011) Sustained superhydrophobic friction reduction at high liquid pressures and large flows. *Langmuir* 27(1):487–493
- Carlborg CF, Do-Quang M, Stemme G, Amberg G, van der Wijngaart W (2008) Continuous flow switching by pneumatic actuation of the air lubrication layer on superhydrophobic microchannel walls. In: Proceedings of the 21st IEEE international conference on micro electro mechanical systems. IEEE, Tucson, pp 599–602
- Cassie ABD, Baxter S (1944) Wettability of porous surfaces. *Trans Faraday Soc* 40:546–551
- Cheng YP, Teo CJ, Khoo BC (2009) Microchannel flows with superhydrophobic surfaces: effects of Reynolds number and pattern width to channel height ratio. *Phys Fluids* 21:122004
- Choi CH, Kim CJ (2006a) Large slip of aqueous liquid flow over a nanoengineered superhydrophobic surface. *Phys Rev Lett* 96:066001
- Choi CH, Kim CJ (2006b) A reply to the comment on ‘Large slip of aqueous liquid flow over a nanoengineered superhydrophobic surface’. *Phys Rev Lett* 97:109602
- Choi CH, Westin KJA, Breuer KS (2003) Apparent slip flows in hydrophilic and hydrophobic microchannels. *Phys Fluids* 15:2897–2902
- Choi CH, Ulmanella U, Kim J, Ho CH, Kim CJ (2006) Effective slip and friction reduction in nanogated superhydrophobic microchannels. *Phys Fluids* 18:087105
- Cottin-Bizonne C, Barrat JL, Bocquet L, Charlaix E (2003) Low-friction flows of liquid at nanopatterned interfaces. *Nat Mater* 2:237–240
- Cottin-Bizonne C, Barentin C, Charlaix E, Bocquet L, Barat JL (2004) Dynamics of simple liquids at heterogeneous surfaces: molecular-dynamics simulations and hydrodynamic description. *Eur Phys J E* 15:427–438
- Cottin-Bizonne C, Barentin C, Bocquet L (2012) Scaling laws for slippage on superhydrophobic fractal surfaces. *Phys Fluids* 24:012001
- Daniello RJ, Waterhouse NE, Rothstein JP (2009) Drag reduction in turbulent flows over superhydrophobic surfaces. *Phys Fluids* 21:085103
- Davies J, Maynes D, Webb BW, Woolford B (2006) Laminar flow in a microchannel with superhydrophobic walls exhibiting transverse ribs. *Phys Fluids* 18:087110
- Davis AMJ, Lauga E (2009a) The friction of a mesh-like superhydrophobic surface. *Phys Fluids* 21:113101
- Davis AMJ, Lauga E (2009b) Geometric transition in friction for flow over a bubble mattress. *Phys Fluids* 21:011701
- Davis AMJ, Lauga E (2010) Hydrodynamic friction of fakir-like superhydrophobic surfaces. *J Fluid Mech* 661:402–411
- Feuillebois F, Bazant MZ, Vinogradova OI (2009) Effective slip over superhydrophobic surfaces in thin channels. *Phys Rev Lett* 102:026001

- Gao P, Feng JJ (2009) Enhanced slip on a patterned substrate due to depinning of contact line. *Phys Fluids* 21:102102
- Genzer J, Efmenko K (2006) Recent developments in superhydrophobic surfaces and their relevance to marine fouling: a review. *Biofouling* 22:339–360
- Gogte S, Vorobieff P, Truesdell R, Mammoli A, van Swol F, Shah P, Brinker CJ (2005) Effective slip on textured superhydrophobic surfaces. *Phys Fluids* 17:051701
- Govardhan RN, Srinivas GS, Asthana A, Bobji MS (2009) Time dependence of effective slip on textured hydrophobic surfaces. *Phys Fluids* 21:052001
- Hendy SC, Lund NJ (2007) Effective slip boundary conditions for flows over nanoscale chemical heterogeneities. *Phys Rev E* 76:066313
- Holt JK, Park HG, Wang Y, Stadermann M, Artyukhin AB, Grigoriopoulos CP, Noy A, Bakajin O (2006) Fast mass transport through sub-2-nanometer carbon nanotubes. *Science* 312:1034–1037
- Hyvalouma J, Harting J (2008) Slip flow over structured surfaces with entrapped microbubbles. *Phys Rev Lett* 100:246001
- Joseph P, Tabeling P (2005) Direct measurement of an apparent slip length. *Phys Rev E* 71:035303
- Joseph P, Cottin-Bizonne C, Benoit JM, Ybert C, Journet C, Tabeling P, Bocquet L (2006) Slippage of water past superhydrophobic carbon nanotube forests in microchannels. *Phys Rev Lett* 97:156104
- Jung YC, Bhushan B (2010) Biomimetic structures for fluid drag reduction in laminar and turbulent flows. *J Phys: Condens Matter* 22:035104
- Karatay E, Hasse AS, Visser CW, Sun C, Lohse D, Tsai PA, Lammertink RGH (2013) Control of slippage with tunable bubble mattresses. *Proc Natl Acad Sci* 110(21):8422–8426
- Kashaninejad N, Nguyen NT, Chan WK (2012) Eccentricity effects of microhole arrays on drag reduction efficiency of microchannels with a hydrophobic wall. *Phys Fluids* 24:112004
- Kim TJ, Hidrovo C (2012) Pressure and partial wetting effects on superhydrophobic friction reduction in microchannel flow. *Phys Fluids* 24:112003
- Kim D, Hwang W (2010) A template-based superhydrophobic tube structure with nanofiber forests and its mass flow characteristic. *J Micromech Microeng* 20:027002
- Kim J, Kim CJ (2002) Nanostructured surfaces for dramatic reduction of flow resistance in droplet-based microfluidics. In: *Proceedings of the 15th IEEE international conference on micro electro mechanical system. IEEE, Las Vegas*, pp 479–482
- Kim CJ, Wudl F, Ho CM, Garrell RL (2002) NanoTurf and NanoPebbles: Toward zero-flow friction surfaces. In: *Booklet of NSF Nanoscale Science and Technology Grantee Conference, Arlington, VA, USA, Dec 2002*, http://www.nseresearch.org/2002/Grantees02_Program1208.htm
- Lauga E, Stone HA (2003) Effective slip in pressure-driven Stokes flow. *J Fluid Mech* 489:55–77
- Lauga E, Brenner MP, Stone HA (2005) In: *Foss CTJ, Yarin A (eds) Handbook of experimental fluid dynamics*, chap. 15. Springer, Berlin
- Lee C, Kim CJ (2009) Maximizing the giant liquid slip on superhydrophobic microstructures by nanostructuring their sidewalls. *Langmuir* 25(21):12812–12818
- Lee C, Kim CJ (2011a) Influence of surface hierarchy of superhydrophobic surfaces on liquid slip. *Langmuir* 27(7):4243–4248
- Lee C, Kim CJ (2011b) Underwater restoration and retention of gases on superhydrophobic surfaces for drag reduction. *Phys Rev Lett* 106:014502
- Lee C, Kim CJ (2012) Wetting and active dewetting processes of hierarchically constructed superhydrophobic surfaces fully immersed in water. *J Microelectromech Syst* 21(3):712–720
- Lee A, Kim HY (2014) Does liquid slippage within a rough channel always increase the flow rate? *Phys Fluids* 26:072002
- Lee Y, Yong K (2015) Combining the lotus leaf effect with artificial photosynthesis: regeneration of underwater superhydrophobicity of hierarchical ZnO/Si surfaces by solar water splitting. *NPG Asia Mater* 7:e201
- Lee C, Choi CH, Kim CJ (2008) Structured surfaces for a giant liquid slip. *Phys Rev Lett* 101:064501
- Lee DJ, Cho KY, Jang S, Song YS, Youn JR (2012) Liquid slip on a nanostructured surface. *Langmuir* 28:10488–10494
- Li J, Zhou M, Ye X, Cai L (2010) Self-comparison measurement for slippage on superhydrophobic surfaces based on the wetting transition. *J Micromech Microeng* 20:115022
- Liu T, Kim CJ (2015) Turning a surface super-repellent even to completely wetting liquids. *Science* 346:1096–1100
- Lu Y, Sathasivam S, Song J, Crick CR, Carmalt CJ, Parkin IP (2015) Robust self-cleaning surfaces that function when exposed to either air or oil. *Science* 347:1132–1135
- Maali A, Pan Y, Bhushan B, Charlaix E (2012) Hydrodynamic drag-force measurement and slip length on microstructured surfaces. *Phys Rev E* 85:066310
- Martell MB, Perot JB, Rothstein JP (2009) Direct numerical simulations of turbulent flows over superhydrophobic surfaces. *J Fluid Mech* 620:31–41
- Martell MB, Rothstein JP, Perot JB (2010) An analysis of superhydrophobic turbulent drag reduction mechanisms using direct numerical simulation. *Phys Fluids* 22:065102
- Maynes D, Jeffs K, Woolford B, Webb BW (2007) Laminar flow in a microchannel with hydrophobic surface patterned microribs oriented parallel to the flow direction. *Phys Fluids* 19:093603
- Ming Z, Jian L, Chunxia W, Lan C (2011) Fluid drag reduction on superhydrophobic surfaces coated with carbon nanotube forests (CNTs). *Soft Matter* 7:4391–4396
- Neto C, Evans DR, Bonaccorso E, Butt HJ, Craig VSJ (2005) Boundary slip in Newtonian liquids: a review of experimental studies. *Rep Prog Phys* 68:2859–2897
- Ng CO, Wang CY (2009) Stokes shear flow over a grating: implications for superhydrophobic slip. *Phys Fluids* 21:013602
- Ng CO, Wang CY (2010) Apparent slip arising from Stokes shear flow over a bidimensional patterned surface. *Microfluid Nano-fluidics* 8:361–371
- Nizkaya TV, Asmolov ES, Vinogradova OI (2014) Gas cushion model and hydrodynamic boundary conditions for superhydrophobic textures. *Phys Rev E* 90:043017
- Ou J, Rothstein JP (2005) Direct velocity measurements of the flow past drag-reducing ultrahydrophobic surfaces. *Phys Fluids* 17:103606
- Ou J, Perot B, Rothstein JP (2004) Laminar drag reduction in microchannels using ultrahydrophobic surfaces. *Phys Fluids* 16(12):4635–4643
- Park H, Park H, Kim J (2013) A numerical study of the effects of superhydrophobic surface on skin-friction drag in turbulent channel flow. *Phys Fluids* 25:110815
- Park H, Sun G, Kim CJ (2014) Superhydrophobic turbulent drag reduction as a function of surface grating parameters. *J Fluid Mech* 747:722–734
- Philip JR (1972a) Flows satisfying mixed no-slip and no-shear conditions. *Z Angew Math Phys* 23:353–372
- Philip JR (1972b) Integral properties of flows satisfying mixed no-slip and no-shear conditions. *Z Angew Math Phys* 23:60–968
- Poetes R, Holtzmann K, Franze K, Steiner U (2010) Metastable underwater superhydrophobicity. *Phys Rev Lett* 105:166104
- Priezjev NV, Darhuber AA, Troian SM (2005) Slip behavior in liquid films on surfaces of patterned wettability: comparison between continuum and molecular dynamics simulations. *Phys Rev E* 71:041608
- Quééré D (2005) Non-sticking drops. *Rep Prog Phys* 68:2495–2532

- Richardson A (1973) On the no-slip boundary condition. *J Fluid Mech* 59:707–719
- Sakai M, Nakajima A, Fujishima A (2010) Removing an air layer from a superhydrophobic surface in flowing water. *Chem Lett* 39:482–484
- Samaha MA, Tafreshi HV, Gad-el-Hak M (2011) Modeling drag reduction and meniscus stability of superhydrophobic surfaces comprised of random roughness. *Phys Fluids* 23:012001
- Sbragaglia M, Prosperetti A (2007a) A note on the effective slip properties for microchannel flows with superhydrophobic surfaces. *Phys Fluids* 19:043603
- Sbragaglia M, Prosperetti A (2007b) Effective velocity boundary condition at a mixed slip surface. *J Fluid Mech* 578:435–451
- Schäffel D, Koynov K, Vollmer D, Butt HJ, Schönecker C (2016) Local flow field and slip length of superhydrophobic surfaces. *Phys Rev Lett* 116:134501
- Shirtcliffe NJ, McHale G, Newton MI, Zhang Y (2009) Superhydrophobic copper tubes with possible flow enhancement and drag reduction. *ACS Appl Mater Interface* 1:1316–1323
- Solomon BR, Khalil KS, Varanasi KK (2014) Drag reduction using lubricant-impregnated surfaces in viscous laminar flow. *Langmuir* 30:10970–10976
- Srinivasan S, Choi W, Park KC, Chhatre SS, Cohen RE, McKinley GH (2013) Drag reduction for viscous laminar flow on spray-coated non-wetted surfaces. *Soft Matter* 9:5691–5702
- Steinberger A, Cottin-Bizonne C, Kleimann P, Charlaix E (2007) High friction on a bubble mattress. *Nat Mater* 6:665–668
- Teo CJ, Khoo BC (2008) Analysis of Stokes flow in microchannels with superhydrophobic surfaces containing a periodic array of micro-grooves. *Microfluid Nanofluidics* 7:353–382
- Teo CJ, Khoo BC (2010) Flow past superhydrophobic surfaces containing longitudinal grooves: effects of interface curvature. *Microfluid Nanofluidics* 9:499–511
- Truesdell R, Mammoli A, Vorobieff P, van Swol F, Brinker CJ (2006) Drag reduction on a patterned superhydrophobic surface. *Phys Rev Lett* 97:044504
- Tsai P, Peters AM, Pirat C, Wessling M, Lammertink RGH, Lohse D (2009) Quantifying effective slip length over micropatterned hydrophobic surfaces. *Phys Fluids* 21:12002
- Vakarelski IU, Chan DYC, Thoroddsen ST (2014) Leidenfrost vapor layer moderation of the drag moderation of the drag crisis and trajectories of superhydrophobic and hydrophilic spheres falling in water. *Soft Matter* 10:5662–5668
- Vinogradova OI, Belyaev AV (2011) Wetting, roughness and flow boundary conditions. *J Phys: Condens Matter* 23:184104
- Wang Y, Bhushan B (2010) Boundary slip and nanobubble study in micro/nanofluidics using atomic force microscopy. *Soft Matter* 6:29–66
- Wang Y, Bhushan B, Maali A (2009) Atomic force microscopy measurement of boundary slip on hydrophilic, hydrophobic, and superhydrophobic surfaces. *J Vac Sci Technol, A* 27:754–760
- Wang Q, Li J, Zhang C, Qu X, Liu J, Yang Z (2010) Regenerative superhydrophobic coating from microcapsules. *J Mater Chem* 20:3211–3215
- Watanabe K, Udagawa Y, Udagawa H (1999) Drag reduction of Newtonian fluid in a circular pipe with a highly water-repellent wall. *J Fluid Mech* 381:225–238
- Watanabe K, Takayama T, Ogata S, Isozaki S (2003) Flow between two coaxial rotating cylinders with a highly water-repellent wall. *AIChE J* 49:1956–1963
- Wenzel RZ (1936) Resistance of solid surfaces to wetting by water. *Ind Eng Chem* 28:988–994
- Westin KJA, Choi CH, Breuer KS (2003) A novel system for measuring liquid flow rates with nanoliter per minute resolution. *Exp Fluids* 34:635–642
- Wexler JS, Jacobi I, Stone HA (2015) Shear-driven failure of liquid-infused surfaces. *Phys Rev Lett* 114:168301
- Wong TS, Kang SH, Tang SKY, Smythe EJ, Hatton BD, Grinthal A, Aizenberg J (2011) Bioinspired self-repairing slippery surfaces with pressure-stable omniphobicity. *Nature* 477:443–447
- Xu M, Sun G, Kim CJ (2014) Infinite lifetime of underwater superhydrophobic states. *Phys Rev Lett* 113:136103
- Ybert C, Barentin C, Cottin-Bizonne C, Joseph P, Bocquet L (2007) Achieving large slip with superhydrophobic surface: scaling laws for generic geometries. *Phys Fluids* 19:123601